Mohammed A. Mohammed [1]
Khansaa N. Aklo [2]
Anaam W. Watan [2]
Kareem A. Jasim [2]
Ebtisam M-T. Salman [2]

[1] *Department of Remote Sensing and GIS, College of Science, University of Baghdad, Baghdad, IRAQ*
[2] *Department of Physics, College of Education for Pure Sciences / Ibn Al-Haitham, University of Baghdad, Baghdad, IRAQ*

Effect of Thermal Neutron Radiation Dose on Density of Local and Extended Energy States in $Se_{55}S_{20}Sb_{15}Sn_{10}$ Alloy

Four samples of the $Se_{55}S_{20}Sb_{15}Sn_{10}$ alloy were prepared using the melting point method. Samples B, C and D were irradiated with (6.04×10^{10}, 12.08×10^{10} and 18.12×10^{10} ($n.cm^{-2}s^{-1}$) of thermal neutron beam from a neutron source (241Am-9Be) respectively, while sample A was left not irradiated. The electrical properties were assessed both before and after the radiation. All irradiated and non-irradiated samples show three conduction mechanisms, at low temperatures, electrical conductivity is achieved by electron hopping between local states near the Fermi level. At intermediate temperatures, conduction occurs by the jumping of electrons between local states at band tails. At high temperatures, electrons transfer between extended states in bands. The results show that the local and extended state densities above the Fermi level are affected by exposure to thermal neutron radiation.

Keywords: Melt quenching; Thermal neutron beam; Electron hopping
Received: 03 January 2024; **Revised:** 02 March; **Accepted:** 09 March 2024

1. Introduction

Studies on the properties of amorphous chalcogenide semiconductors have shown that, due to the presence of local states close to the Fermi level and in the energy gap, where the Fermi level was pinned, they generally behave as doping-insensitive P-type semiconductors [1-3]. It was found that the amorphous chalcogenides might be improved for use in device applications by substituting certain chemical components entirely or with metallic impurities [4]. This increased their conductivity and greatly lowered the conduction activation energy [5]. According to Mott, any element may satisfy the valence criterion in chalcogenides applying the 8-N rule [6]. The electrical and optical properties of doped chalcogenides don't vary much because this rule holds for doped elements. The researchers demonstrated that adding atoms of some chemical elements (such as bismuth) to chalcogenide glass causes a significant change in the p-type electrical conductivity of more than 7% compared to that of the n-type [7]. In contrast, the addition of other elements (like In, Sb, Sn) always indicates a p-type compound [8,9]. Since not all impurities can be electroactive, the concentration of the impurities is undoubtedly a key element in such situations [10,11]. It is therefore important, both from the point of view of basic research and applied research, to investigate the influence of impurities on the properties of chalcogenide glass [12,13].

The electrical characteristics of the chalcogenide glass are significantly altered when impurity atoms are added to the Se-Te-Sn and Ge-Te-Sb binary systems, according to the findings of multiple experimental investigations [14]. In addition, the composition of the glass, the chemistry of the impurities, and the doping technique have a significant impact on the behavior of the chalcogenide glass [15]. This study investigated the density of the extended, local, and Fermi levels of In and their effects of indium on the $Se_{85}Te_{10}Sn_{5-x}In_x$. These include changes to the activation energy, tail width, and distance between states in addition to a decrease in the density of extended and local states, also known as Fermi states [14]. When the Sb element in the $Ge_{30}Te_{70-x}Sb_x$ alloy was partially exchanged, the density of local and extended states, as well as the Fermi level, were examined, and it was discovered that all energy states, including activation energy, tail width, interatomic distances, and transition distance, changed [15]. The studies [10-13] focused on examining the electrical characteristics of $Se_6Te_{4-x}Sb_x$ and $Se_6Te_{4-x}Sn_x$ alloys by partially replacing Te with Sb and the energy density was calculated for several energy states, including electron hopping distance, Fermi level, localization, and tail width. They concluded that the states of energy density increase along with the concentration of Sb. One of the distinctive characteristics of amorphous chalcogenide semiconductors is their susceptibility to the effects of external factors, notably ionizing radiation with an average energy of more than 1 MeV [16,17].

To gain additional knowledge regarding how radiation affects dc conductivity measurements at various temperatures and to exploit amorphous chalcogenides in electrical device applications. We

will investigate the impact of thermal neutron irradiation on the random energy level and crystal regularity of $Se_{55}S_{20}Sb_{15}Sn_{10}$ samples, as well as the densities of states (local, extended, and Fermi levels). This paper will be finished to exploit amorphous chalcogenides in electrical device applications.

2. Experimental Part

Four samples of $Se_{55}S_{20}Sb_{15}Sn_{10}$ alloy (A, B, C and D) were prepared by melt-cooling technique. The raw material powders of high purity Se, S, Sb, and Sn (99.99%) were weighed according to the atomic weight ratios. The mixture was mixed using an electric mill to obtain a homogeneous powder. After the mixture was put into a quartz glass tube and evacuated to 10^{-4} Torr, the tube was securely sealed. This was done to remove any impurities from the capsule and ensure that it could resist the pressure created by the alloy's constituent chemical elements interacting with one another without blowing apart within the furnace due to the high temperature. Seal the ampoule hermetically. To prevent selenium from precipitating on the inner wall of the quartz tube and from evaporating suddenly, the ampoule was then heated in two phases. Three hours were spent gradually heating and holding the ampoule at 500 °C. For seven hours, the furnace's temperature was increased to 960°C at a rate of 6°C per minute. To get the glassy state, the ampoule was quickly chilled with ice-cooled water. The sample powder was then extracted by grinding the resulting ingot using a pestle and mortar. The powder was divided into four parts, and the powder was pressed for each of these parts using a hydraulic press with a pressure of 5 tons per square cm to obtain the tablets (A, B, C and D) with a diameter of one and a half centimeters and a thickness of 5mm. Continuous electrical conductivity was measured as a function of temperature within the room temperature range up to 227°C for sample A, and samples B, C and D were subjected to a thermal neutron beam with different doses (6.04×10^{10}, 12.08×10^{10}, 18.12×10^{10} n.cm^{-2}s^{-1}). For the irradiation samples (B, C, and D), the continuous electrical conductivity was evaluated as a function of temperature within the room temperature range up to 227°C, and then theoretical calculations were made on the results of electrical conductivity before and after irradiation using computer software.

3. Results and Discussion

The electrical (I-V) measurements were carried out at different temperatures (from 22 to 207 °C) to observe how the direct current electrical conductivity of $Se_{55}S_{20}Sb_{15}Sn_{10}$ alloy's glass. The electrical resistivity and then the electrical conductivity were calculated for all samples. All values of electrical conductivity of the samples were calculated about temperature. Based on testing the $Se_{55}S_{20}Sb_{15}Sn_{10}$ alloy's electrical resistance before and after exposure to thermal neutron beam radiation.

To demonstrate the relationship between continuous electrical conductivity and temperature changes, figure (1) shows the relationship between electrical conductivity ln(σ) and temperature. It is noted from this figure that all samples of the alloy $Se_{55}S_{20}Sb_{15}Sn_{10}$ before and after exposure to irradiation behave like semiconductors (that is, they have an electrical conductivity that increases with temperature in an exponential relationship) [18,19].

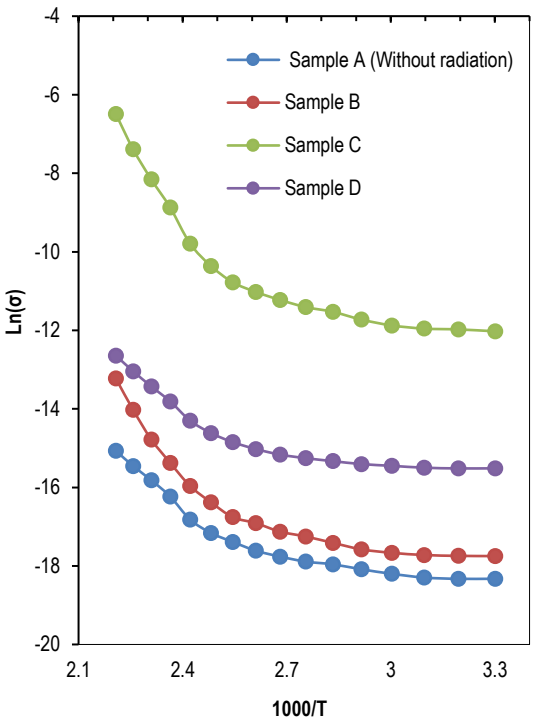

Fig. (1) Electrical conductivity plot (Ln σ) for $Se_{55}S_{20}Sb_{15}Sn_{10}$ samples as a function of temperature sample A without irradiation. Samples B, C and D were irradiated with doses of 6.04×10^{10}, 12.08×10^{10}, 18.12×10^{10} n.cm^{-2}, respectively

Additionally, it is shown that, in general, continuous electrical conductivity rises whenever subjected to a thermal neutron beam; however, sample C (dose 12.08×10^{10} n.cm^{-2}) has been significantly impacted in comparison to samples B and D (dose 6.04×10^{10} and 18.12×10^{10} n.cm^{-2}s^{-1}). This behavior in electrical conductivity explains that the alloys were affected when they collided with thermal neutrons, which led to their acquisition of additional energy by rearranging the atoms. The alloy had the best energy absorbed by the sample, while less or more than this dose, the conductivity increased slightly [16].

Figure (1) depicts the relationship between temperature and dc electrical conductivity for all glass samples $Se_{55}S_{20}Sb_{15}Sn_{10}$ both before and after irradiation. Additionally, each sample's curve reveals three distinct conduction regions at low, medium, and high temperatures, indicating the existence of three distinct electrical conduction mechanisms [10,11]. It was found that the conductivity increases slowly from 22 to 72 °C and increases remarkably quickly beyond

72 to 122 °C, and then the conductivity increases rapidly when the temperature is increased from 122 to 207 °C. The charge carriers gain energy when the temperature rises from 22 to 72 °C, and conduction happens as a result of the carriers in the local states jumping in the ranges near the Fermi level. The low temperature also results in low obtained conduction energy [14,20]. The conductivity is shown to rise as a result gradually. However, the charge carriers become more mobile above 22 K, and conduction happens as a result of the charge carriers leaping in the band tails. As a result, conduction is anticipated to occur by variable mobility (VRH) in the lower temperature range (122 to 207 °C). In contrast, in the higher temperature range (72 to 122 °C), as demonstrated in Fig. (1), conductivity increases, and conduction occurs via the thermally assisted process by the transfer of conduction electrons between the stretched states (between the conduction and valence bands this behavior fits Eq. (1) [15,21].

$$\sigma = \sigma_{01} e^{(-\frac{E_1}{KT})} + \sigma_{02} e^{(-\frac{E_2}{KT})} + \sigma_{03} e^{(-\frac{E_3}{KT})} \qquad (1)$$

where ΔE_1, ΔE_2, and ΔE_3 are the activation energies of each term, T is the absolute temperature, and σ_{01}, σ_{02}, σ_{03} are the pre-exponential factor parameters

The slope and intercept of the plot were used in the temperature range of low (22-72°C), middle (72-122°C) and high (122-207°C) to determine the activation energy (E_1, E_2, E_3) and the factor (σ_{01}, σ_{02}, σ_{03}) of $Se_{55}S_{20}Sb_{15}Sn_{10}$ glass, respectively. In table (1), the pre-exponential factor (σ_0) provides important information regarding the conduction process in chalcogenide glass.

The curves demonstrate that there are three separate paths leading to three different slopes produced by three activation energies in thermal activation conduction. According to equation 1, the slope of the plot of ln(σ) against 1000/T can be used to determine the activation energy (E_1, E_2, E_3).

Equation (1) may be used to calculate the pre-exponential factors σ_{01}, σ_{02} and σ_{03} for all samples in the three areas based on the span of the curves and their intersection with the y-axis when the x-axis equals zero. Table (1) shows the values for the pre-exponential factor 0, which were calculated [22]. This figure also, shows that the relationship between lnσ and 1000/T is nonlinear and that the many defects in the grain boundaries that result from insufficient atomic bonding are what cause the changes in electric conduction by enclosing charge carriers in the low-temperature zone and also densities of the state also promote the mobility of the carriers in the high-temperature area because they lower the trapping state and potential barrier [23,24]. There is no doubt that the electrical conductivity after the neutron radiation improved more quickly than the compound without neutron radiation. The density of states near the Fermi level, therefore, starts to change. We will use the activation energies (E_1, E_2, E_3), the exponential factor parameters ((σ_{01}, σ_{02}, σ_{03}) and the width of the tails that were calculated from the relation ($\Delta E=E_2-E_1$) of each part of the curves shown in Eq. (1) and written in tables (1) and (2) to determine the densities of local and extended states for each sample before and after irradiation.

Figure (2) depicts the correlation between the energy tail width values ($\Delta E=E_1-E_2$) and the thermal neutron radiation dosage. This graph illustrates the variation in the amplitude of the energy tail values between samples that were exposed to thermal neutron radiation doses of 6.04×10^{10}, 12.08×10^{10}, and 18.12×10^{10} n.cm^{-2}s^{-1} and without irradiation sample. This suggests that the radiation had an impact on the density of the energy levels inside the samples' mobility gaps, this modification results from the samples' crystal recombination as a result of their absorption of radiation energy [16,17].

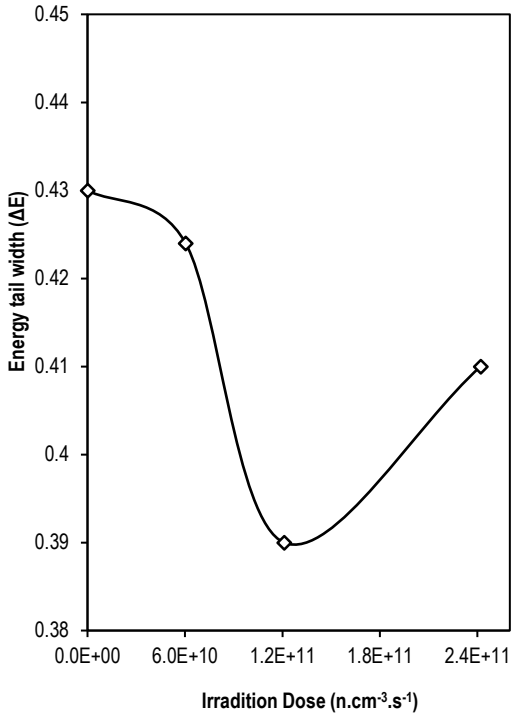

Fig. (2) Energy tail width ΔE values plot for $Se_{55}S_{20}Sb_{15}Sn_{10}$ as a function of thermal neutron irradiation dose

To calculate the energy state densities in three different regions – localized $N(E_{loc})$, extended $N(E_{ext})$, and Fermi level $N(E_F)$ after and before irradiation. After substituting the values of the constants (electron charge e, the electron mass and the values σ_{01}, σ_{02}, σ_{03} into the equations in references [13,14] mentioned below the energy state density was calculated in three different regions—local, extended, and Fermi level. The results are recorded in table (2).

$$N(E_{ext}) = [\frac{6m}{e^2\hbar}]\sigma_{0ext} \qquad (2)$$

where ħ = 1.0545×10^{-34} J.s

$$N(E_{loc}) = [\frac{6}{e^2 V_{ph} \hbar R^2}]\sigma_{0loc} \quad (3)$$

where V_{ph} is the phonon frequency, which is of order 10^{13} $s^{-1}$and R is the hopping distance and is given by

$$R = 0.7736[\frac{\Delta E a^{-1}}{N(E_C)(KT)^2}]^{0.25}$$

and

$$\gamma^{-1} = 10 \text{ A}$$

$$N(E_F) = [\frac{6}{e^2 V_{ph} \hbar R^2}]\sigma_{03} \quad (4)$$

It is noted from table (2) and Fig. (3) the intensity of the values of the stretched state ($N_{(Eext)}$), the density of the stretched state increases from the value 1.5×10^{18} $eV^{-1}cm^{-3}$ for the non-irradiated sample to 3.94×10^{19}, 5.78×10^{20} and 3.62×10^{19} $eV^{-1}cm^{-3}$ at a radiation dose with thermal neutrons of 6.04×10^{10}, 12.08×10^{10}, 18.12×10^{10} $n.cm^{-2}s^{-1}$, respectively. It can be seen from Fig. (3) that the density of extended states ($N_{(Eext)}$) increases with increasing radiation dose and the greatest value is at sample C. This is due to an increase in radiation energy, which may occur for several reasons, such as change in the value of the mobility gap, width of the E tails, concentration of conductors, or a shift in the conductor [12,18,19].

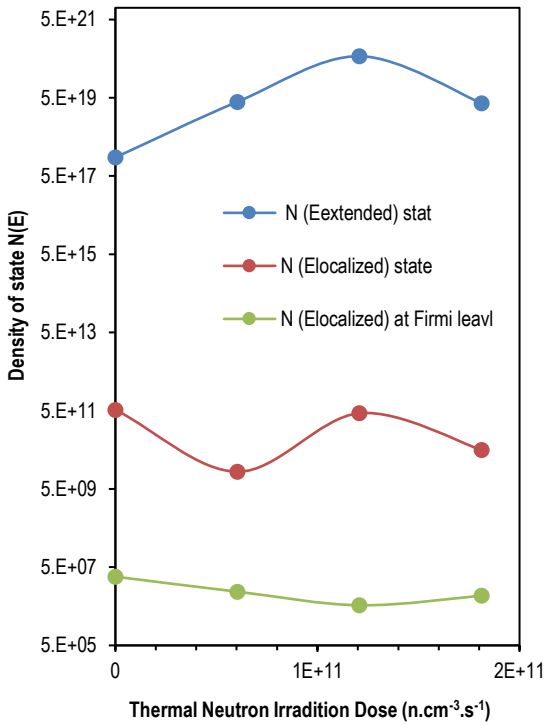

Fig. (3) Densities of energy states in localized, extended and Fermi level regions plot for $Se_{55}S_{20}Sb_{15}Sn_{10}$ as a function of thermal neutron irradiation dose

The local state density determined by Eq. (3) can also be calculated as table (2) and figure (3) note how the thermal neutron radiation dose affects it [18]. As for the local state density, it was before irradiation 5.28×10^{11} $eV^{-1}cm^{-3}$ for sample A, and it decreased after irradiation, and it was 1.38×10^{10}, 4.32×10^{11}, and 4.94×10^{10} $eV^{-1}cm^{-3}$ for samples B, C and D at a radiation dose of 6.04×10^{10}, 12.08×10^{10}, 18.12×10^{10} $n.cm^{-2}s^{-1}$, respectively, as shown in Fig. (3) and table (2). The transition of the alloy's crystalline structure from an amorphous to a crystal state is largely influenced by the rise in the stretched state's density and the fall in the state's density. Polycrystalline means that this behavior has reduced the randomness of the crystal structure of the samples irradiated with thermal neutrons [16].

To determine the localized state density around the Fermi level $N(E_F)$ for all samples before and after radiation, we substitute the parameter values of the pre-exponential factor σ_{03} and the jump distance R in the low-temperature region into Eq. (4) and write the results in table (2).

From Fig. (3) and table (2), it can be seen that the densities of local states close to the Fermi level decrease with the increase in the dose of thermal neutrons, where the value was recorded as 2.85×10^{7} $eV^{-1}cm^{-3}$ before radiation and became 1.18×10^{7}, 5.3×10^{6} and 9.32×10^{6} $eV^{-1}cm^{-3}$ after radiation for samples B, C and D respectively.

4. Conclusions

The effects of thermal neutron radiation exposure on the density of localized, extended, and localized Fermi level states in melting-quenched $Se_{55}S_{20}Sb_{15}Sn_{10}$ alloy were studied. When determining electrical conductivity, three conduction pathways are discovered, indicating the existence of extended, local, and Fermi-level states at low, medium, and high temperatures, where it was found that all of these densities of states are unmistakably affected by variations in the dose of thermal neutron radiation. The width of the energy tails, the hopping distance of the electrons, as well as the activation energy all vary with the radiation dose.

References

[1] N. Tohge, H. Matsuo and T. Minami, "Electrical properties of n-type semiconducting chalcogenide glasses in the system Pb-Ge-Se", *J. Non-Cryst. Solids*, 95 (1987) 809-816.

[2] N. Tohge, K. Kanda and T. Minami, "Formation of chalcogenide glass p-n junctions", *Appl. Phys. Lett.*, 48(25) (1986) 1739-1741.

[3] R.A Street and N.F. Mott, "States in the gap in glassy semiconductors", *Phys. Rev. Lett.*, 35(19) (1975) 1293.

[4] N.F. Mott, "Introductory talk; Conduction in non-crystalline materials", *J. Non-Cryst. Solids*, 8 (1972) 1-18.

[5] K.A. Shore, "Electronic processes in non-crystalline materials", 2nd ed., N.F. Mott and E.A. Davis, *Contemp. Phys.*, 55(4) (2014) 337.

[6] S.P. Vikhrov, P. Nagels and P.K. Bhat, "n-Type Conduction in Chalcogenide Glasses of the Ge-Se-Bi System", *Recent Develop. Cond. Matter*

Phys.: vol. 2, Metals, Disordered Systems, Surfaces, and Interfaces, Springer (NY, 1981), 333-340.

[7] N. Tohge, T. Minami and M. Tanaka, "Photoconductivity of vitreous chalcogenides chemically modified by bismuth", *J. Non-Cryst. Solids*, 59 (1983) 999-1002.

[8] J.S. Mohammed et al., "Investigating the optical and electrical characteristics of $As_{60}Cu_{40-x}Se_x$ thin films prepared using pulsed laser deposition method", *Chalcogen. Lett.*, 20(7) (2023) 449-458.

[9] K.A. Jasim, S.A. Makki and A.A. Almohsin, "Comparison Study of Transition Temperature between the Superconducting Compounds $Tl_{0.9}Pb_{0.1}Ba_2Ca_2Cu_3O_{9-\delta}$, $Tl_{0.9}Sb_{0.1}Ba_2Ca_2Cu_3O_{9-\delta}$ and $Tl_{0.9}Cr_{0.1}Ba_2Ca_2Cu_3O_{9-\delta}$", *Phys. Procedia*, 55 (2014) 336-341.

[10] B.A. Ahmed et al., "The dependence of the energy density states on the substitution of chemical elements in the $Se_6Te_{4-x}Sb_x$ thin film", *Chalcogen. Lett.*, 19(4) (2022) 301-308.

[11] N.H. Khudhair and K.A. Jasim, "Study the effect of tin on the energy density of states of $Se_{60}Te_{40-x}Sn_x$ chalcogenide glass", *AIP Conf. Proc.*, 2769(1) (2023) 020062.

[12] N.H. Khudhair and K.A. Jasim, "Preparation and study the effective of Sb on the energy density of states of $Se_{60}Te_{40}$", *AIP Conf. Proc.*, 2769(1) (2023) 020056.

[13] N.H. Khudhair and K.A. Jasim, "A Study of the Effectiveness of Tin on the Thermal Conductivity Coefficient and Electrical Resistance of $Se_{60}Te_{40-x}Sn_x$ Chalcogenide Glass", *Ibn Al-Haitham J. Pure Appl. Sci.*, 36(1) (2023) 149-157.

[14] A.N. Abdulateef et al., "Calculating the Mechanisms of Electrical Conductivity and Energy Density of States for $Se_{85}Te_{10}Sn_{5-x}In_x$ Glasses Materials", *J. Green Eng.*, 10 (2020) 5487-5503.

[15] R.K. Chillab et al., "Fabrication of $Ge_{30}Te_{70-x}Sb_x$ Glasses Alloys and Studying the Effect of Partial Substitution on D.C Electrical Energy Parameters", *Key Eng. Mater.*, 900 (2021) 163-171.

[16] K.A. Jasim et al., "The effect of neutron irradiation on the properties of $Tl_{0.6}Pb_{0.3}Cd_{0.1}Ba_2Ca_2Cu_3O_{9-\delta}$ superconductors", *Turkish J. Phys.*, 37(2) (2013) 237-241.

[17] Z.J. Neamah et al., "The effect of gamma radiation on the manufactured $HgBa_2Ca_2Cu_{2.4}Ag_{0.6}O_{8+\delta}$ compound", *Mater. Sci. Forum*, 1050 (2022) 41-47.

[18] D. Adler, (1975). **"Disordered materials: Amorphous and liquid Semiconductors"**. J. Tauc (ed.), Plenum Press (NY, 1974), p. 442.

[19] J.K. Lee et al., "Control of thermoelectric properties through the addition of Ag in the $Bi_{0.5}Sb_{1.5}Te_3$ alloy", *Electron. Mater. Lett.*, 6 (2010) 201-207.

[20] M. Mobarak, H.T. Shaban and A.F. Elhady, "Electrical and thermoelectric properties of $CuInS_2$ single crystals", *Mater. Chem. Phys.*, 109(2-3) (2008) 287-290.

[21] H.A. Mahdi, K.A. Jasim and A.H. Shaban, "Manufacturing and improving the characteristics of the isolation of concrete composites by additive Styrofoam particulate", *Energy Procedia*, 157 (2019) 158-163.

[22] D.K. Paul and S.S. Mitra, "Evaluation of Mott's parameters for hopping conduction in amorphous Ge, Si, and Se-Si", *Phys. Rev. Lett.*, 31(16) (1973) 1000.

[23] K.A. Jassim, W.H. Jassim and S.H. Mahdi, "The effect of sunlight on medium density polyethylene Water pipes", *Energy Procedia*, 119 (2017) 650-655.

[24] D.J. Thouless, "Disordered materials: Electronic processes in non-crystalline Materials", N.F. Mott and E.A. Davis (ed.), 2nd ed., Clarendon (Oxford University Press), (NY, 1979), p. 590.

Table (1) Activation energies (ΔE_1, ΔE_2, ΔE_3) and values of (σ_{01}, σ_{02} and σ_{03}) are dependence on Neutron radiation of $Se_{55}S_{20}Sb_{15}Sn_{10}$ sample after and radiation

Neutron Dose ($n.cm^{-2}.s^{-1}$)	ΔE_1	σ_{oext}	ΔE_2	σ_{oLoc}	ΔE_3	σ_{ofermi}
0	0.43	4.66×10^{-4}	0.142	2.27×10^{-2}	0.0879	1.52×10^{-8}
6.04×10^{10}	0. 424	1.22×10^{-3}	0.242	9.22×10^{-2}	0.0168	9.25×10^{-6}
12.08×10^{10}	0. 39	1.79×10^{-3}	0.231	7.078×10^{-1}	0.0547	1.68×10^{-6}
18.12×10^{10}	0.41	$1.1\,2\times 10^{-3}$	0.217	3.54×10^{-1}	0.063	1.85×10^{-7}

Table (2) Tail width ΔE, a, R, N (E_{ext}), N (E_{loc}) and N(E_F) of $Se_{55}S_{20}Sb_{15}Sn_{10}$ alloy dependent on the of thermal neutron Irradiation Dose

Neutron Dose ($n.cm^{-2}.s^{-1}$)	ΔE (eV)	R A^0	a A^0	$N_{(Ext)}$ ($eV^{-1}cm^{-3}$)	$N_{(Eloc)}$ ($eV^{-1}cm^{-3}$)	$N_{(EF)}$ ($eV^{-1}cm^{-3}$)
0	0.288	2.7	1.45	1.5×10^{18}	5.28×10^{11}	2.85×10^{7}
6.04×10^{10}	0.182	2.8	1.16	3.94×10^{19}	1.38×10^{10}	1.18×10^{7}
12.08×10^{10}	0.159	1.08	1.09	5.78×10^{20}	4.32×10^{11}	5.3×10^{6}
18.12×10^{10}	0.193	3.30	1.215	3.62×10^{19}	4.94×10^{10}	9.32×10^{6}

